RAL-TR-2000-022

Energy Resolution in X-ray Detecting Gas Microstrip Detectors

J.E.Bateman, J.F.Connolly, G.E.Derbyshire, D.M.Duxbury, J.A.Mir, E.J.Spill and R. Stephenson

Rutherford Appleton Laboratory, Chilton, Didcot, Oxon, OX11 0QX, UK

12 June 2000

Abstract

Systematic measurements of the energy resolution available from a Gas Microstrip Detector (GMSD) are presented. The effect of factors such as bias potential, gas filling and strip geometry on the energy resolution are examined in detail and related to a simple model. The geometry of the GMSD is adapted to permit “wall-less” detection of x-rays and this results in useful improvements in the pulse height spectra.

1. Introduction

At Rutherford Appleton Laboratory we are developing various Gas Microstrip Detectors (GMSD) for application to experimental techniques which utilise x-ray beams from Synchrotron Radiation Sources (SRS). Among these are detectors for the measurement of X-ray Absorption Fine Structure (XAFS) using both the auger [1] and soft x-ray [2] emissions and for the measurement of Small and Wide Angle X-ray Scattering data (SAXS/WAXS) [3]. The capability of these detectors to count at high data rates and resolve x-ray positions to sub-millimetre accuracy has been explored and reported [1-3]; in this report the energy resolving capabilities of the GMSD are investigated in the context of x-ray spectrometry.

As a gas counter, the energy resolution of the GMSD will always remain inferior to that of semiconductor detectors in the x-ray region. However, the ability of the GMSD to combine energy resolution with very high data capture rates and sub-millimetre spatial resolution makes it possible to use it to separate elements in an (emission) XAFS study or select auger electrons in a surface analysis study. It has been shown elsewhere that the peculiar structure of the GMSD (with all the gain-defining electrodes on a single rigid plane) permits flexible application to materials analysis [1]; in this study the advantages of this structure for the optimisation of the energy resolution are examined.

2. The Gas Microstrip X-ray Detector

The GMSD x-ray detector [4] consists of a suitable semi-insulating substrate patterned with an array of appropriately biased metal electrodes which intercept and amplify the x-ray-generated electron clouds which drift down from a conversion space defined by a drift electrode placed parallel to the GMSD plate (figure 1). In the present tests the electrode pattern is produced lithographically in either gold or chromium on S8900 glass plates which are 50mm square. In one design, anode strips of 10μm width are interleaved with cathode strips of 90μm on a repeat pitch of 300μm. The anodes and cathodes are bussed in groups of twenty giving seven independent detector sections of active area 12mm x 6mm. The gas containment vessel is configured so that the x-rays can enter parallel to the plate surface into the drift region defined by a conductive foil electrode placed 10mm from the plate. A second design of plate maintains the basic dimensions as above with the exception that the anode width is varied between values of 2, 3, 4 and 5μm in the different sections of the counter.

The anode groups are held near earth potential with independent negative EHT supplies connected to the cathodes (V_c) and the drift electrode (V_d). The anodes can be instrumented with a slow amplifier (CR-RC time constants of 1.5μs) for connection to a Pulse Height Analyser (PHA) or with faster amplifier circuits (100ns time constants) for connection to discriminators and logic circuits. With a typical gas atmosphere of argon +25% isobutane operating potentials are $V_c \approx -700V$, $V_d \approx -1500V$ with the detector delivering a gas gain of ≈1500. Low noise charge preamplifiers (1000 electrons RMS) minimise the gain demanded from the GMSD.

A gas mixing system permits the use of a wide (and closely controlled) range of gas atmospheres within the counter, permitting great flexibility in the x-ray operating energy range.

3. X-ray Energy Resolution in the GMSD

The basic processes of x-ray conversion and avalanche gain in the GMSD are essentially the same as in the single wire cylindrical proportional counter about which a large literature exists. This is reviewed well in reference 5 and the following analysis is based on the standard concepts described therein.

In the cylindrical wire counter the drift electric field (near the cathode) and the avalanche field (near the anode) are part of the same field pattern. Figure 2 shows that the typical electric field pattern in the GMSD is divided into two well-defined regions – the drift region of essentially constant field and the intense avalanche region near the anode. The latter is limited in extent to within approximately one pitch (of the strip pattern) from the plate. In the case of the GMSDs under test this is only 3% of the drift depth. This gives rise to the useful simplification that (to first order) the gas gain (M) is dependent only on the anode-cathode potential difference (Vc) and the drift field (E_d) only on V_d-V_c. In fact there are small interactions which are encompassed by the finding that M depends on the potential $Vc + \alpha V_d$ where α is ≈0.007 for most of the permutations of gas and geometry used in these tests [1] and $E_d \approx (V_d - 0.7V_c)/L$ (L is the drift depth) for the typical geometry of the present GMSDs. The latter relation is found experimentally (see below) and represents the fact that the leakage of the dipole field from the plate into the gap is $\approx 0.3V_c/L$.

The dispersion of the recorded signal in the counter can be evaluated in terms of the variance introduced by several independent processes; the final variance is then taken as the sum of the individual variances.

1. Ionisation. When an x-ray of energy E_x interacts with a gas atom in the drift space it produces a fast electron (usually by the photoelectric process) which ionises a large number of gas atoms releasing a number of electrons N_e. N_e is evaluated in terms of the mean energy required to make an ion pair in the gas w, so that $N_e = E_x / w$. The value of w is relatively independent of the gas (or gas mixture) in use so that 25eV < w < 30eV. For a mixture of argon + 25% isobutane the value of w is close to 27eV.

   The variance in N_e is found to be FN_e where F is the Fano factor and, for argon-based mixtures is measured to be 0.17. Amplified by the avalanche process this variance appears as a contribution $\sigma_1^2 = M^2 F N_e$ to the variance of the final number of electrons in the anode pulse.

2. Avalanche Multiplication: The quasi-punctual cloud of electrons drifts towards the anode structures where the high electric field induces multiplication. Each electron generates its own avalanche which belongs to a typical distribution called the Single Electron Response Function (SERF). If the variance of the SERF is σ_{se}^2 then the variance induced in the amplified electron signal is $\sigma_2^2 = M^2 N_e \sigma_{se}^2$, where we have assumed that all the ionisation signal N_e reaches the anode. The theoretical model of Alkhazov [7] indicates that $0.6 < \sigma_{se}^2 < 0.8$ in the operating

range typical with GMSDs.

3. Geometric Uniformity: The gas gain is a sensitive function of the electric field through which the avalanche propagates. Thus geometric fluctuations in the definition of the electrodes (particularly the anode) impose a variance on the anode signals as the incident x-ray beam covers a considerable length of anode. In one detector, for example, the RMS fluctuation in the width of a 4μm wide anode was 128nm (3.2%). Such fluctuations are very dependent on the processing of the GMSD and the resulting gain fluctuations over the active area (σ_g) are variable but rarely greater than 2% RMS. The geometric gain variance shows up in the final anode signal as $\sigma_3^2=(MN_e\sigma_g)^2$.

4. Amplifier Noise: Since the gain available from GMSDs is relatively restricted (a few thousand) it is important to use a low noise amplifier system. The low stray capacity of the anodes (≈0.2pF/cm of anode length) makes it comparatively easy to attain noise figures of 1000 electron RMS (σ_e) with fast pulse-shaping times. This noise appears directly in the anode electron signal: $\sigma_4^2=\sigma_e^2$.

5. Electron attachment: The assumption made (in section 2) above that all the primary electrons reach the avalanche region is often not met in practice due to the attachment of some of the electrons to electronegative impurities during the drift. Electron attachment is an extremely complex process in which small concentrations of certain electronegative impurities (e.g. oxygen) can interact with the other gas components in a catalytic manner to produce rather severe electron losses (an effect used in smoke detectors). Efficient electron transport requires that the electrons be moved to the anode before significant losses can occur; hence it is a sharp function of the drift field.

   The loss of the primary signal can be characterised by an attachment length λ_a. In a drift distance l the signal is attenuated by a factor of $exp(-l/\lambda_a)$. In x-ray counters the x-rays are generally absorbed (more-or-less) uniformly throughout the drift distance L. This leads to a distribution of pulse heights spread over a range $MN_e(1-exp(-L/\lambda_a)$. The mean of this distribution is $MN_e\lambda_a/L(1-exp(-L/\lambda_a)$ and the standard deviation is $0.288MN_e\{1-exp(-L/\lambda_a)\}$. It follows that $\lambda_a = v\tau$ where v is the drift velocity of the electrons and τ is the lifetime of the free electrons against attachment. At low values of the drift field (E_d) both the drift velocity and the lifetime are rapid functions of the field strength (τ is inversely proportional to the attachment coefficient – see reference 8 for a discussion) and both tend to level off at high drift fields.

   The well-defined, and accessible drift region of the GMSD means that (as will be shown below) λ_a can be measured directly as a function of V_d. Thus we can define a further contribution to the variance sum: $\sigma_5^2=\{0.288MN_e(1-exp(-L/\lambda_a(E_d))\}^2$, where E_d is as defined above.

6. Electron Drift Path Variation: The gas gain is defined by the relation

$$\ln M = \int \alpha_T dr \qquad (1)$$

where α_T is the Townsend coefficient (a strong function of the electric field) and the integral takes place along the path followed by the electron on its approach to the anode through the region of high field. In the field configuration depicted in figure 2 (which corresponds to a low drift field) it is clear that all electrons from the drift space well above the plate follow a narrow cone of paths into the anode. It is this geometry which enables the GMSD to give good energy resolution in spite of the complex field pattern near the anode. The modelling of the gain process in a GMSD presented in reference [9] shows that if an electron originates in the space immediately above the cathode, it can (when one integrates up equation (1)) experience a gain of approximately double that of electrons approaching the anode directly from above the anode.

Two effects can cause x-ray clouds (or parts of them) to get into this region. First, x-rays may convert directly in this region. In general this is a small contribution because the depth of the region is about one half of a pitch of the electrode pattern (i.e. in our case 1/60 of the total drift depth) and cathodes form only about 50% of the area of the plate. So for uniform radiation of the detector (with low drift field) one might expect to see a tail of about 1% of pulses up to nearly twice the peak pulse height.

The second mechanism capable of delivering drifting electrons into the cathode "hot spot" occurs when the drift field is increased. The field configuration of figure 2 now shifts and an increasing number of field lines from the drift region are pulled in to the cathode hot spot. Since diffusion in the drift makes the initial electron cloud spread out by more than a strip pitch in a 1 cm drift (even in the gases with the lowest diffusion) the electrons can easily "jump" field lines and be diverted into the hot spot on their way to the anode. This effect leads to the growth of a high energy tail on the x-ray pulse height distribution as V_d is raised.

The effects of the cathode hot spot are impossible to model simply and also produce a severely skewed distribution. Accordingly this contribution to the total signal variance will be left simply symbolically as σ_6^2.

The variance of the anode electron signal is thus: $\sigma^2 = \Sigma\sigma_n^2$. In experimental work it is usual to work in terms of the relative full width at half maximum of the x-ray peak expressed as a percentage (*FWHM*). This is defined by $FWHM^2 = 236^2\sigma^2/(MN_e)^2$. Thus:

$$FWHM^2 = 236^2[F/N_e + \sigma_{se}^2/N_e + \sigma_g^2 + \sigma_e^2/(MN_e)^2 + 0.288^2\{1-\exp(-L/\lambda_a)\}^2] \quad (2)$$

Here the simplification of neglecting the effect of the attachment loss on the primary electron and avalanche statistics is made (the validity this is confirmed by the experimental data). The effect of the cathode hot spot is neglected in equation (2) because the low amplitude tail generated by this process has a negligible effect at the half height of the x-ray peak. In equation (2) M is principally dependent on V_c and λ_a on V_d.

The dependence of the *FWHM* on the x-ray energy becomes explicit if we substitute $N_e=E_x/w$ in equation (2). Thus:

$$FWHM^2 = 236^2[(F + \sigma_{se}^2)w/E_x + \sigma_g^2 + \sigma_e^2w^2/(ME_x)^2 + 0.288^2\{1-\exp(-L/\lambda_a)\}^2] \quad (3)$$

4. Energy Resolution Measurements

Figure 3 shows a typical pulse height spectrum recorded by 5.9keV x-rays in a one section (6mm wide) GMSD operating with a filling of Ar + 25% isobutane. With a *FWHM* of ≈16% one observes the full energy and argon escape peak with a background of small pulses due to wall effects and obvious signs of a high energy tail due to the effects discussed above in the context of the cathode hot spot. Direct measurements of the *FWHM* are made for the data presented below.

4.1 Measurements of the *FWHM* as a function of the Gain (*M*)

Figure 4 shows a plot of the *FWHM* of the 5.9keV x-ray peak in one 6mm section of a GMSD with an argon + 25% isobutane mixture. The drift potential (V_d = -1300V) is optimised to minimise the fourth term in equation (3) (see below for explanation) and with the "wall" events suppressed (see below for explanation). Under these conditions the fit parameter *b* picks out term number three with the sum of the remaining terms evaluated as the fit parameter *a*. Since $b = \sigma_e w/E_x = 5.12$, using E_x=5900eV and w=27eV/ion pair gives σ_e=1119eV for the RMS amplifier noise.

The significance of figure 4 is that with an amplifier noise figure of ≈1000 electrons RMS, this term becomes insignificant at gas gains of >1000. In other words, the relatively low gas gains of the GMSD (relative to wire counters) do not limit the energy resolution. The asymptotic *FWHM* defined by the remaining term (*a*) is 14.1%.

4.2 Measurements of the *FWHM* as a function of the Drift Potential (V_d)

Figure 5 shows the results when the *FWHM* is measured as a function of the drift potential. There is an initial reduction in the *FWHM* followed by a small rise. The initial decrease is clearly due to the rapid increase of λ_a with drift field, showing that term 4 in equation (3) becomes negligible (in this case) at a very low V_d. The increase in the energy resolution at higher drift potentials is better characterised by the full width at tenth maximum (*FWTM*) of the peak (figure 5). This shows up the skewing effects of the "cathode hot spot" term.

In order to model the attachment effects, an experimental measurement of λ_a is required. In order to do this a pencil beam of x-rays of 1mm diameter was injected into the drift space of a GMSD parallel to the plate. The peak of the pulse height distributions was measured as a function of V_d with the beam close to the drift electrode and then close to the plate. The ratio of the amplitudes was then taken to represent $exp(-L/\lambda_a)$ where *L* is 1cm in this case. Figure 6 shows the resulting plot of λ_a as a function of $V_d - V_c$. The data fits well to the function $\lambda_a=0.00185(V_d+330.4)^{1.4}$ cm, and λ_a increases from 6.8cm to 103cm over the working range of V_d. The offset of 330V represents the effect of the leakage field from the dipole field of the plate electrodes. From this data it was concluded that a reasonable parameterisation of L/λ_a would be of the form $c/(V_d-0.7V_c)^{1.5}$. This is obviously approximate since the above data is measured in CO_2 while various combinations of argon and quencher are used elsewhere.

4.2.1 Measurements of *FWHM* versus V_d with different gas mixtures

Figure 7 shows the behaviour of the *FWHM* versus V_d plots as the fraction of isobutane in an argon-based mixture is varied in a GMSD with 10μm anodes. At high isobutane concentrations the *FWHM* deteriorates severely and very large drift potentials are required to reach the optimum. Using the model developed above for λ_a and the function derived for the variance of the attachment distribution, the descending parts of the curves can be fitted with the function $FWHM^2=a^2+(236*0.288)^2(1-exp(-c/(V_d-0.7V_c)^{1.5})$, where the parameter a subsumes the non-V_d dependent terms of equation (3) and $c \propto 1/\lambda_a$. As figure 7 shows the fits work quite well permitting the asymptotic resolution and a variable proportional to λ_a to be plotted as a function of the isobutane concentration (figure 8).

In figure 8 it is observed that λ_a exhibits a range of 200 confirming the common experience that pure isobutane is a very electronegative gas. The optimum asymptotic *FWHM* (14.5%) occurs at an isobutane fraction of 25% which is the fraction most commonly used in our GMSDs.

4.2.2 Measurements of *FWHM* versus V_d with variable anode width

There is an expectation (on both theoretical [7] and experimental [10] grounds) that the energy resolution in a gas counter should improve as the anode dimension is reduced. MSGD technology enables one to explore anode dimensions (of a few microns) which are inaccessible to wire counters. Figure 9 shows the *FWHM* versus V_d curves for sections with anode widths (constant within the section of 20 strips) varying between 2μm and 10μm. The gain was ≈700 at V_d=1500V in argon + 25% isobutane. Contrary to expectation, the optimum *FWHM* is obtained with the larger anode widths. Figure 10 shows the same plots in argon + 20% methane. This gas mixture would only deliver stable gas gain of about 50% of that obtainable with an isobutane quencher. This causes the amplifier noise to contribute significantly making the optimum FWHM worse than in isobutane. However, the pattern of the isobutane curves is repeated quite faithfully.

5. Measurements of the Cathode "Hot Spot" Effect

The design of the GMSD allows the distorting effect of the hot spot in the collecting field (positioned just above the cathode strips) to be explored. Using a gas filling of 100% isobutane minimises the diffusion spreading and reduces the spread (during the drift in to the anode) of the electron cloud away from the electric field lines on which it originates. A pencil beam (1mm diameter) of 5.9keV x-rays directed close to the plate (and parallel to it and normal to the strips) ensures the conversion of x-rays in the hot spot and a high drift field (V_d = -4050V across a drift gap of 13mm) ensures that some field lines ending at the anode can scavenge the electrons out of the hot spot. Figure 11a shows the resulting pulse height spectrum in which is observed a very clear secondary peak at 139% of the amplitude of the main peak with ≈12% of the total counts in it. Here clearly is the source of the "high energy tail" observed in the earlier data at high drift fields.

Leaving the beam in the same position while reducing V_d to -1550V produces the PHA spectrum of figure 11b. Here the intensity of the secondary peak is much

reduced (≈5% of the counts) but still evident. In figure 11c the low drift field is maintained while the beam is moved so that it grazes the drift electrode. In this case the intensity of the secondary peak from the hot spot is further reduced to ≈2% as a result of their being very few electron clouds formed on field lines which pass through the hot spot. The counts on the top edge of the peak may, in fact, be compatible with K_β events rather than hot spot counts.

The 13mm drift enforced in figure 11c results in a large fraction of events losing some of their charge to the adjacent strips. This effect is revealed by the large plateau of small pulses stretching from the main peak to the noise.

6. Wall-less Operation

On first creation, the electron cloud generated by an x-ray has a finite dimension due to the range of the photoelectron in the gas. In argon-based mixtures this dimension grows to around 1mm at an x-ray energy of 10keV. As the electron cloud drifts down to the anode, diffusion spreads it out over a gaussian distribution of millimeter dimensions. (in argon +25% isobutane the standard deviation due to 1cm drift is 0.22mm). These two effects result in the loss of some of the energy of the event in the drift cathode/plate and across the edge of the cell defined by a plate section into an adjacent section. If one allows the x-rays to enter the drift gap parallel to the plate, the effects at the drift cathode and the plate surface can be suppressed by collimating the beam so that the edges of the beam remain at least 1mm from the surfaces.

Losses at the edges of the sections can be eliminated by using the adjacent sections as anti-coincidence counters to reject shared events. Since the shared events have the same time structure this anti-coincidence can be performed within a narrow time frame (a few tens of nanoseconds) without inducing significant extra dead time in the counting circuits. Figure 12 shows a high statistics exposure of the Mn 5.9keV x-rays under these conditions in the usual gas mixture. It is clear that the plateau of small pulses seen in figure 3 has completely disappeared. Further, the clean peaks indicate that fitting the peaks with a standard line response function (LRF) should now be possible with a consequent improvement in the identification and quantitation of x-ray lines. The *FWHM* of the 5.9keV peak is not significantly improved by the anti-coincidence system.

The lower discriminator threshold (LLD) in the anti-coincidence sections dictate how well the spectrum is cleaned up. For the Mn lines the spectrum is essentially clean if the LLD is less than 20% of the main peak energy with little improvement below this value. Such LLD levels are easily achieved with gas gains of ≈1000.

Argon-filled gas counters are (in principle) capable of doing spectrometery at x-ray energies of >10keV (all be it with reduced efficiency). However, the long range of the photoelectrons causes wall effects to degrade the energy resolution severely. Wall-less operation (as described above) can ameliorate this situation. Figure 13 shows the PHA spectra recorded when the detector is exposed to an ^{241}Am x-ray fluorescence source with a silver target. Anti-coincidence operation cleans up the spectrum greatly leaving only the fluorescent and Compton-scattered x-rays from the stainless steel source holder. Similar results were obtained with Rb and Mo targets.

7. *FWHM* versus X-ray Energy

The clean-up of the PHA spectra from high energy x-rays (e.g. figure 13) permits the use of the data from the Rb, Mo and Ag K lines to be combined with the Mn data to yield a plot of the *FWHM* versus x-ray energy (E_x) with V_c and V_d constant. This enables the terms dependent on Ex in equation (3) to be evaluated. Figure 14 shows the data with a fit of the appropriate form - $FWHM = sqrt(a^2/E_x^2 + b^2 + c^2/E_x^2)$. It is immediately obvious from figure 14 that the electronic noise term (c^2/E_x^2) is completely negligible and lost in the noise as far as the fit is concerned. The parameter b represents the non-E_x-dependent terms and indicates an asymptotic *FWHM* of 5.14% at large E_x.

From equation (3) we can set $a^2 = 236^2(F + \sigma_{se}^2)w$, where the symbols are as defined above. Setting a= 32.58 (from the fit) F=0.17, and w=27eV, σ_{se}^2 evaluates to 0.536, close to the lower limit (0.6) set by Alkhazov [7].

8. Discussion

The measurements presented above have permitted the characterisation of the energy resolution available from GMSDs within the context of the model represented by equations (2) and (3). Several conclusions regarding the determining factors in the energy resolution are clear:

(i) The electronic noise term (σ_4) is always negligible if the gas gain (M) is around 1000 since the low capacity of the detector makes it possible to have a very low noise preamplifier. For example, if σ_e =1000 electrons its contribution to the *FWHM* of Mn K x-rays is about 0.1% in 14%, i.e. negligible.

(ii) Any geometric non-uniformity (σ_3) of the strip pattern generates a gain variation of σ_g over the active area of the plate (usually from 1 to 100cm^2). Measurements have shown RMS gain variations of between 0.6% and 2% over areas of ≈5cm^2 on differently processed plates. At lower x-ray energies such as the Mn K lines this contribution is small– assuming σ_g = 2% raises a *FHWM* of 14% to 14.8%. However, as figure 14 shows, at higher x-ray energies (>20keV) such an error could come to dominate the FWHM. If high energy x-ray spectroscopy (with, for example, xenon) is contemplated then the quality of the etching becomes important if the intrinsic resolution of the gas processes is to be realised.

(iii) As figure 8 shows, the electron attachment properties of the gas can seriously compromise the *FWHM* available from the GMSD when practical drift distances (e.g. >10mm) are used. Increasing the drift field rapidly lengthens the electron capture length (figure 6) while, unfortunately, increasing the cathode hot spot effect so broadening and skewing the pulse height distribution. The result is a weak minimum in the *FWHM* versus V_d curve and a stronger one in the *FWTM* versus V_d curve (figure 5). In weakly attaching gases this minimum allows the contribution from these effects to be almost negligible. However, as the gas becomes more strongly attaching the minimum in the curve shifts rapidly to the higher V_d and the minimum value of the *FWHM* rises accordingly under the effect of the cathode hot spot. Thus in pure hydrocarbon gases the *FWHM* is generally poorer than in argon mixtures (figure 8).

(iv) The unexpected deterioration of the optimum *FWHM* in a GMSD as the anode with is reduced (figure 9) is interpreted as being due to the increasing dominance of the cathode strip in determining the field pattern near the anode as the anode width is reduced. With the strip geometry employed in the current detectors this effect appears to have a sharp threshold at 4μm anode width. Below this value the cathode hot spot dominates the drift paths of an increasing number of electrons as they approach the anode. It seems clear that around 5μm is the ideal anode width for x-ray spectroscopy.

A repeat study with a filling of Ar + 20% methane showed similar behaviour, with however, generally poorer resolution than with isobutane. The poorer resolution can be interpreted as arising from the larger diffusion coefficient of the methane mixture which allows more electrons to become diverted into the cathode hot spot.

(v) If the electron transport and geometric effects can be eliminated, the resolution of the detector will be determined by the primary electron statistics and the avalanche statistics (σ_1 and σ_2). Using the standard values for argon (F=0.17 and w=27eV) and the measured value of the avalanche variance σ_{se} = 0.536 one finds that the limiting value of the *FWHM* is $FWHM = 32.58 / E_x^{1/2}$. For E_x = 5.9keV this gives *FWHM* = 13.4%, and this value implies that at the optimum V_d and a gain of >1000 the best measured *FWHM* in argon + 25% isobutane of 14.2% (Figure 4) is almost entirely determined by the gas properties. At E_x = 22keV (Figure 14) the gas limit is 6.95% while the measured value is 8.75%. As noted above, this excess is believed to be caused by the geometric non-uniformity of the plate.

The intrinsic limit of the gas processes can be improved by using Penning gas mixtures. (See reference [5] for a review of gas properties.) However, these are very inflexible in composition and very sensitive to pollution, making them quite unsuitable for general use in a high beam environment and over a wide range of x-ray energies.

9. Conclusions

Systematic measurements of the energy resolution of a gas microstrip detector have shown that the electron transport properties of the gas can strongly affect the energy resolution achievable for x-ray lines. If the drift field is chosen carefully the effect of the drift properties can be made negligible for gases with low electron attachment properties and the resolution is determined essentially by the ionisation and avalanche properties of the gas. In general the low gas gain of the GMSD does not degrade the energy resolution.

The simple geometry of the GMSD can be adapted easily to give wall-less operation which radically improves the pulse height spectra available from x-ray lines while preserving the unique ability of the GMSD to divide up the incident beam among a large number of counting channels for high speed data acquisition.

References

1. J.E. Bateman, J.F. Connolly, G.E. Derbyshire, D.M. Duxbury, J. Lipp, J.A. Mir, R. Stephenson, J.E. Simmons and E.J. Spill, Studies of the gain properties of Gas Microstrip Detectors relevant to their application as X-ray detectors, Rutherford Appleton Laboratory Report, RAL-TR-1999-057, (http://www-dienst.rl.ac.uk/library/1999/tr/raltr-1999057.pdf) Presented at the International Workshop on Micro-Pattern Gas Detectors, Orsay, France, 28-30 June 1999.

2. J.E. Bateman, J.F. Connolly, G.E. Derbyshire, D.M. Duxbury, J. Lipp, J.A. Mir, R. Stephenson, J.E. Simmons and E.J. Spill, R.C.Farrow, B.R.Dobson and A.D.Smith, Gas Microstrip X-ray Detectors for Applications in Synchrotron Radiation Experiments, Rutherford Appleton Laboratory Report, RAL-TR-1999-056, (http://www-dienst.rl.ac.uk/library/1999/tr/raltr-1999056.pdf) Presented at the International Workshop on Micro-Pattern Gas Detectors, Orsay, France, 28-30 June 1999.

3. J.E. Bateman, J.F. Connolly, G.E. Derbyshire, D.M. Duxbury, J. Lipp, J.A. Mir, R. Stephenson, J.E. Simmons and E.J. Spill, B.R.Dobson, R.C.Farrow, W. I. Helsby, R. Mutikainen and I. Suni, A Gas Microstrip Wide Angle X-ray Detector for Application in Synchrotron Radiation Experiments, Presented at the 5th International Conference on Position Sensitive Detectors, University College, London, 13-17 September 1999, to be published in Nucl. Instr. & Meth.

4. A. Oed, Nucl. Instr. & Meth. A263 (1988) 351-359

5. G.F.Knoll, Radiation Detection and Measurement, (Chapter 6) John Wiley & Sons, New York, 1989

6. F.Angelini, R.Belazzini, A.Brez, M.M.Massai, G.Spandre, M.R.Torquati, R.Bouclier, J.Gauden and F.Sauli, IEEE Trans. Nucl. Sci.37 (no.2) 1990 112

7. G.D.Alkhazov, Nucl. Instr. & Meth. 89 (1970) 155-165

8. F. Sauli, Principles and operation of multiwire proportional counters and drift chambers, CERN 77-09.

9. T.Beckers, R.Bouclier, Ch. Garabatos, G.Million, F.Sauli, L.I.Shekhtman, Nucl. Instr. & Meth. A346 (1994) 95-101

10. M.A.Fulton, J.J.Kolodziejczak and B.D.Ramsey, Marshall Space Flight Center, Space Science Laboratory preprint 92-118.

Figure Captions

1. Schematic cross-section of a GMSD. The strip pattern runs into the page.

2. A schematic representation of the electric field pattern in the active volume of a gas microstrip detector (adapted from the field plots given in reference [6]). The approximate locations of the cathode "hot-spot" are indicated by the dots.

3. The pulse height distribution generated by 5.9keV x-rays from the anodes of a section of GMSD 6mm wide and 12mm long.

4. The *FWHM* of the Mn K_α x-ray line (from ^{55}Fe) as a function of the gas gain in a section of GMSD operated in "wall-less" mode. Argon + 25% isobutane. Drift potential (V_d) = -1300V, -619<V_c<-460V.

5. The full width at half (*FWHM*) and tenth (*FWTM*) maximum of the pulse height distribution as a function of V_d from a section of GMSD with 2μm wide anodes.

6. The capture length of the drift electrons in a GMSD filled with CO_2.

7. The *FWHM* of the Mn K peak as a function of V_d in a GMSD filled with argon plus a variable fraction of isobutane. The solid curves represent fits based on the model for electron attachment.

8. The fit parameters from figure 7 as a function of the isobutane fraction. *1/c* is proportional to the electron capture length in the gas.

9. The *FWHM* versus V_d plots for GMSD sections with anode widths varying from 2μm to 10μm. The gas filling is argon + 25% isobutane.

10. The *FWHM* versus *Vd* plots for GMSD sections with anode widths varying between 2μm and 4μm. The gas filling is argon + 20% methane.

11. These pulse height spectra show the effect of the cathode hot spot in generating pulses of abnormally large amplitude. (a) With a large drift field and the pencil beam of x-rays close to the plate surface; (b) with a large drift field and the pencil beam close to the drift electrode; (c) with a low drift field and the pencil beam close to the drift electrode. See the text for details.

12. The pulse height spectrum observed from the Mn K lines when a GMSD strip is operated in "wall-less" mode.

13. A comparison of the pulse height spectra observed from an Ag fluorescence source in a section of GMSD with and without "wall-less" operation.

14. A plot of the *FWHM* measured from various x-ray K lines (Mn, Rb, Mo and Ag) as a function of the x-ray line energy.

FIGURE 1

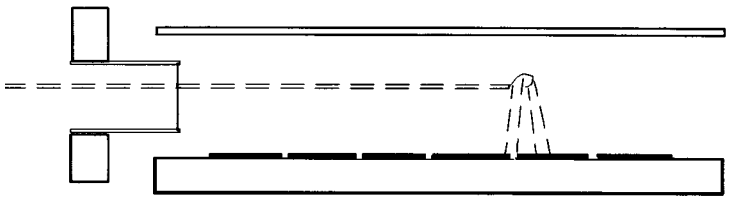

FIGURE 2

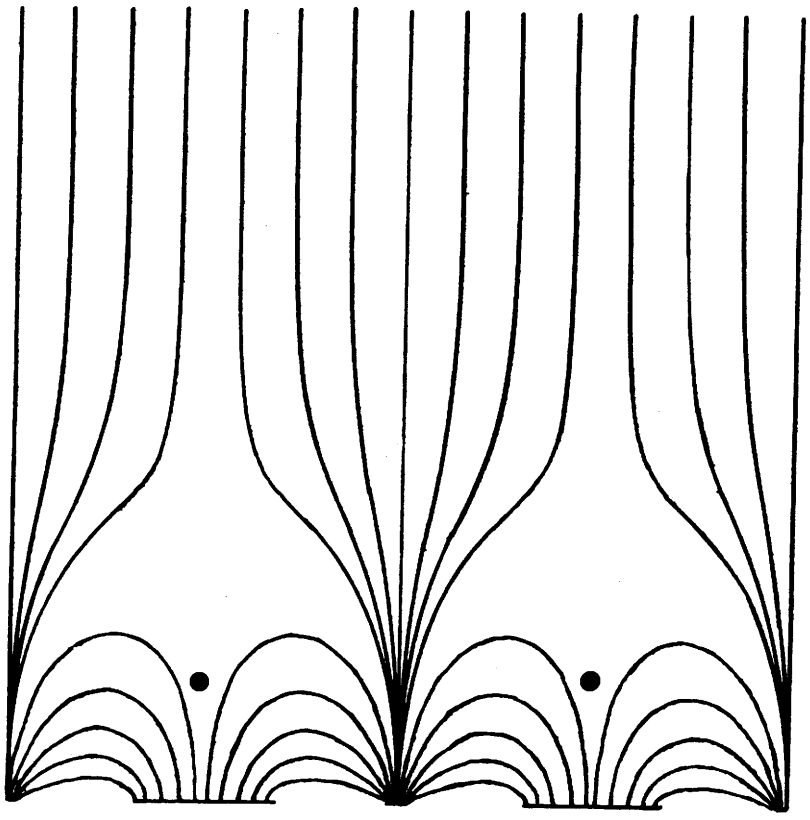

FIGURE 3

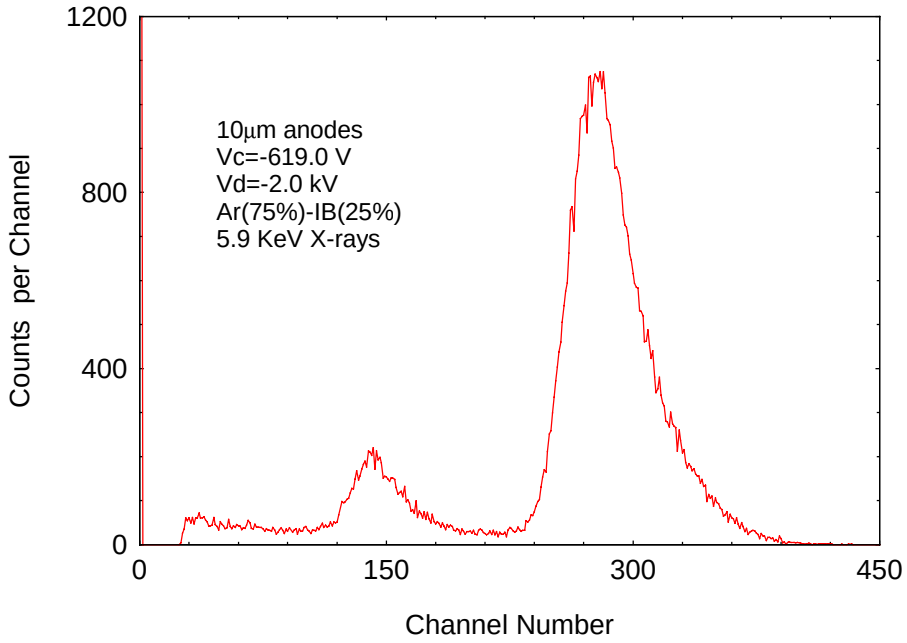

FIGURE 4

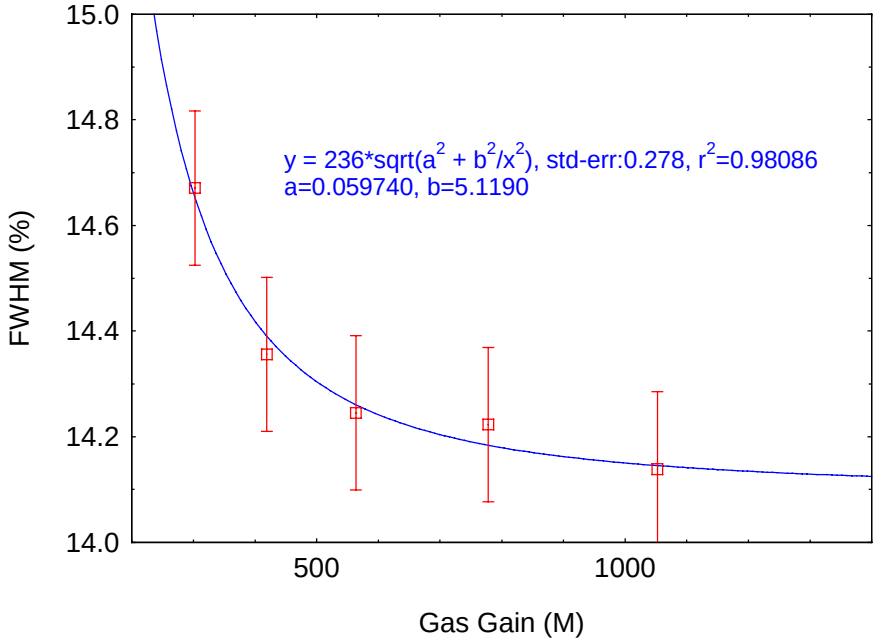

FIGURE 5

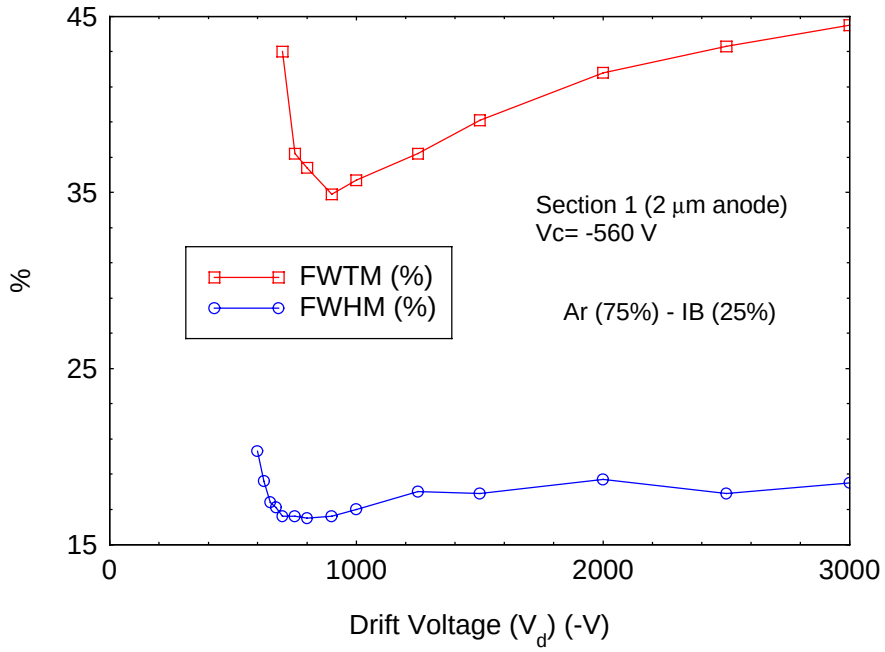

FIGURE 6

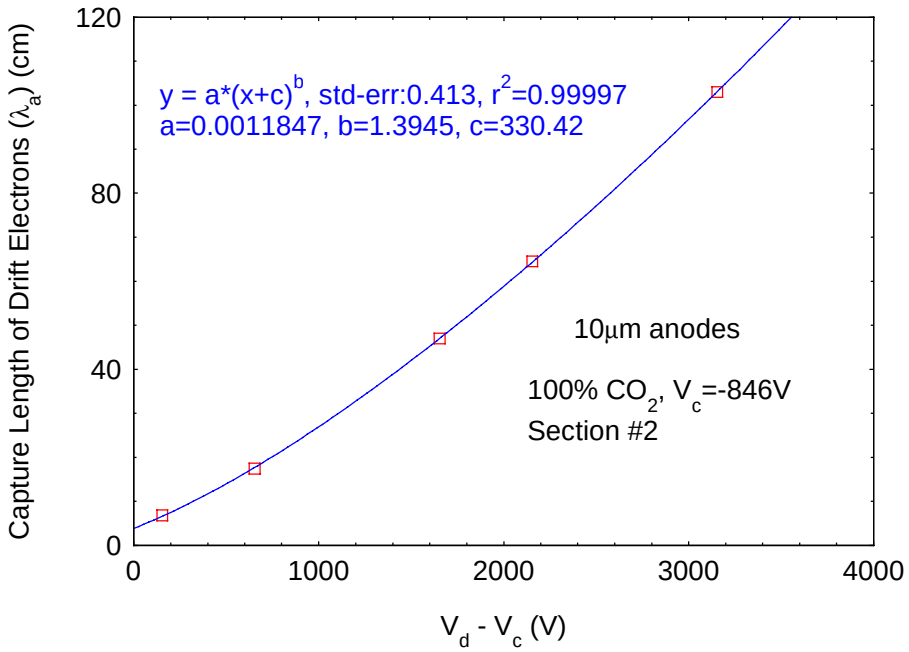

FIGURE 7

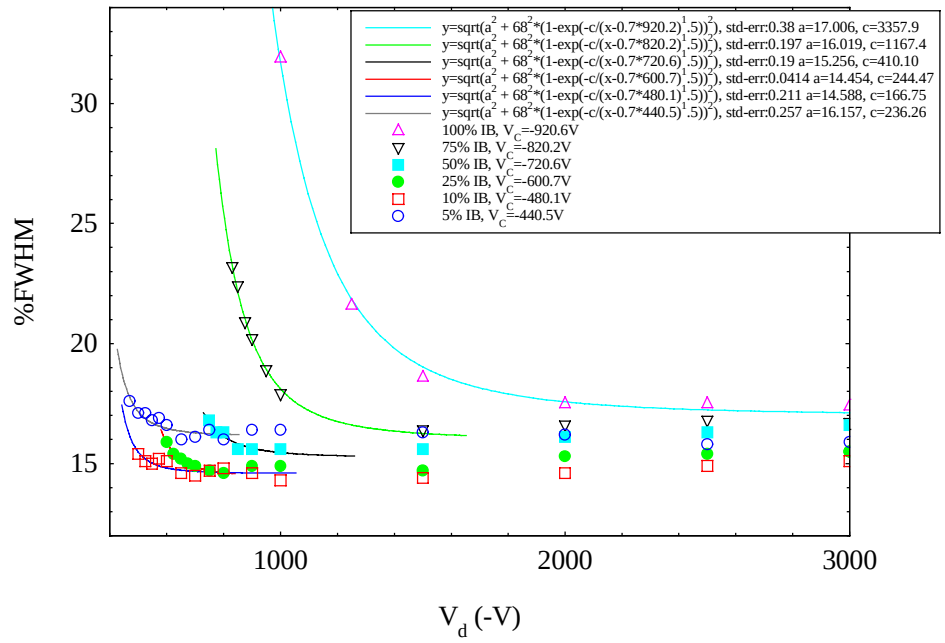

FIGURE 8

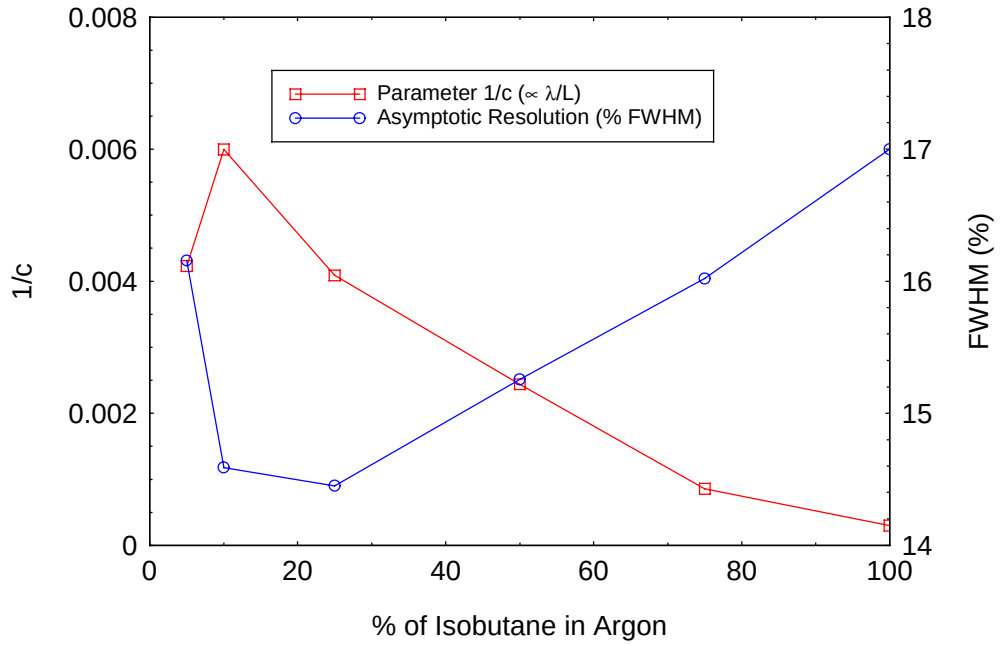

FIGURE 9

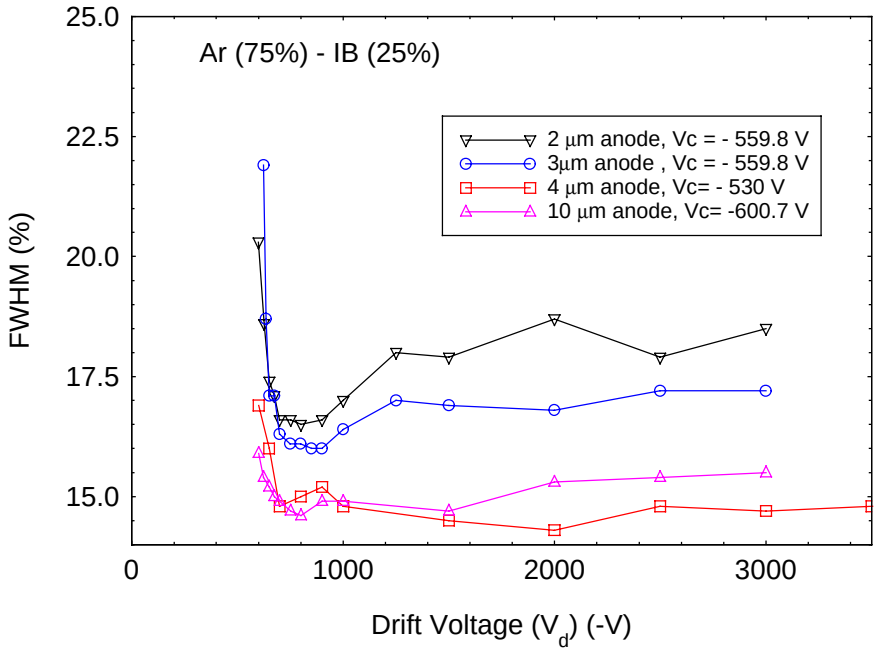

FIGURE 10

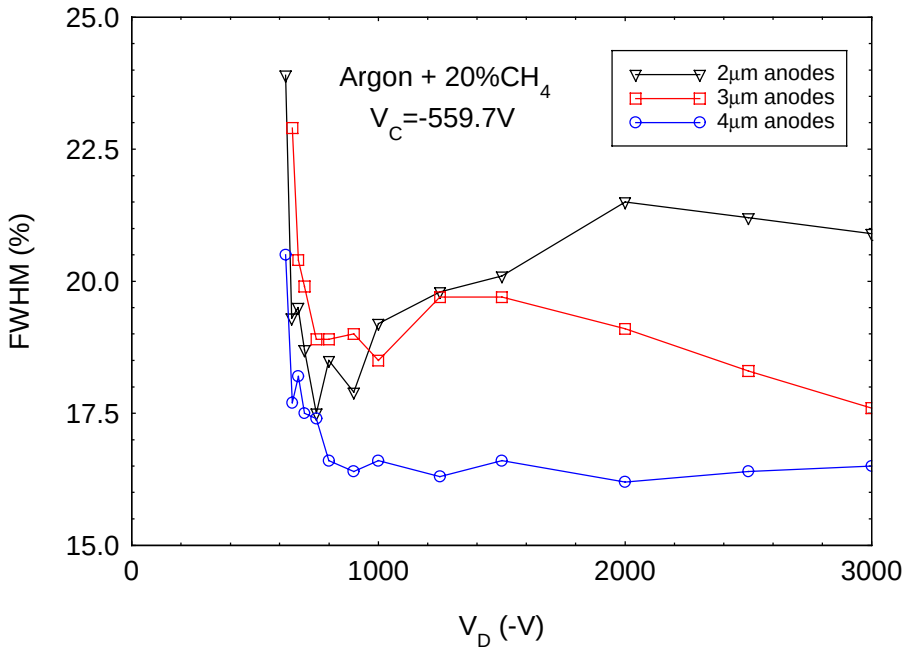

FIGURE 11a

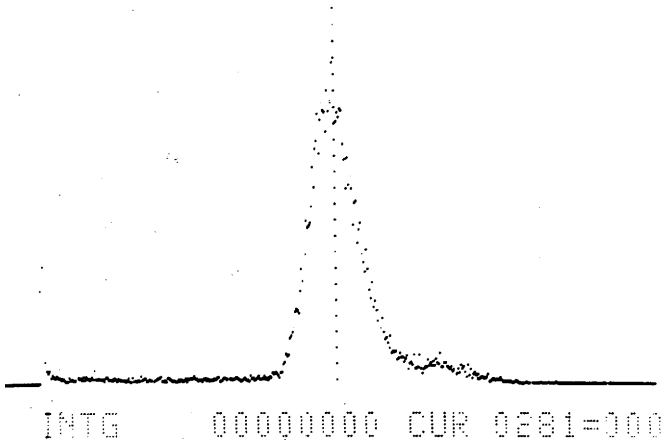

FIGURE 11b

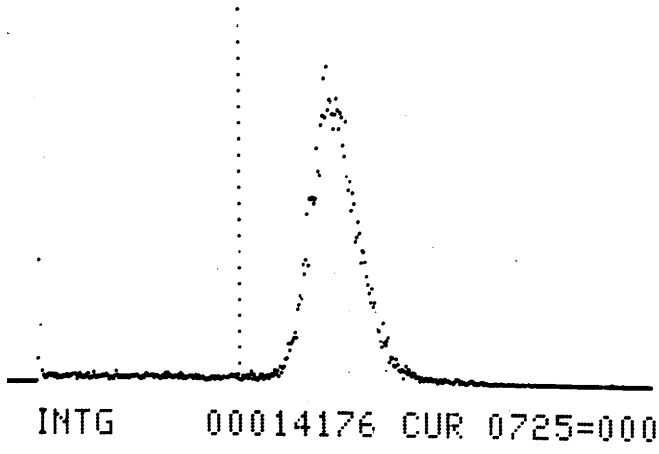

FIGURE 11c

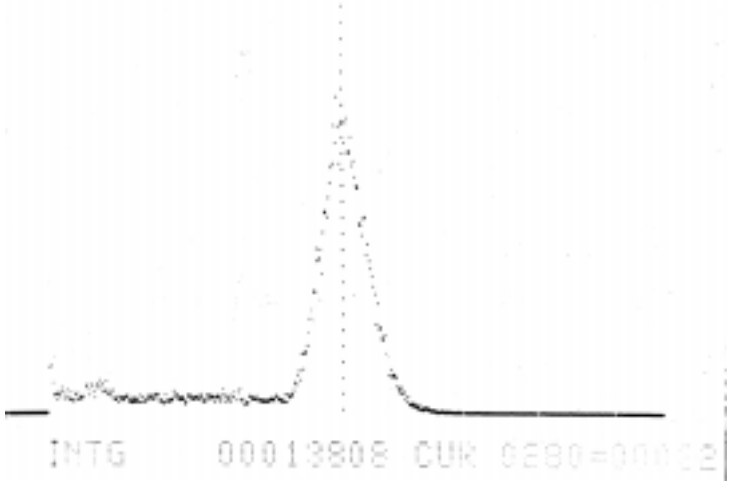

FIGURE 12

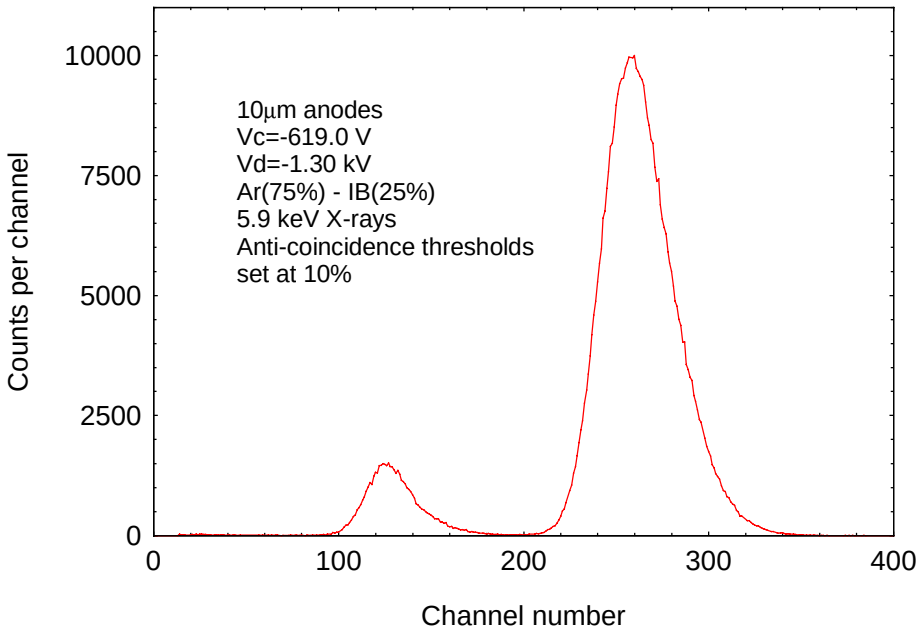

FIGURE 13

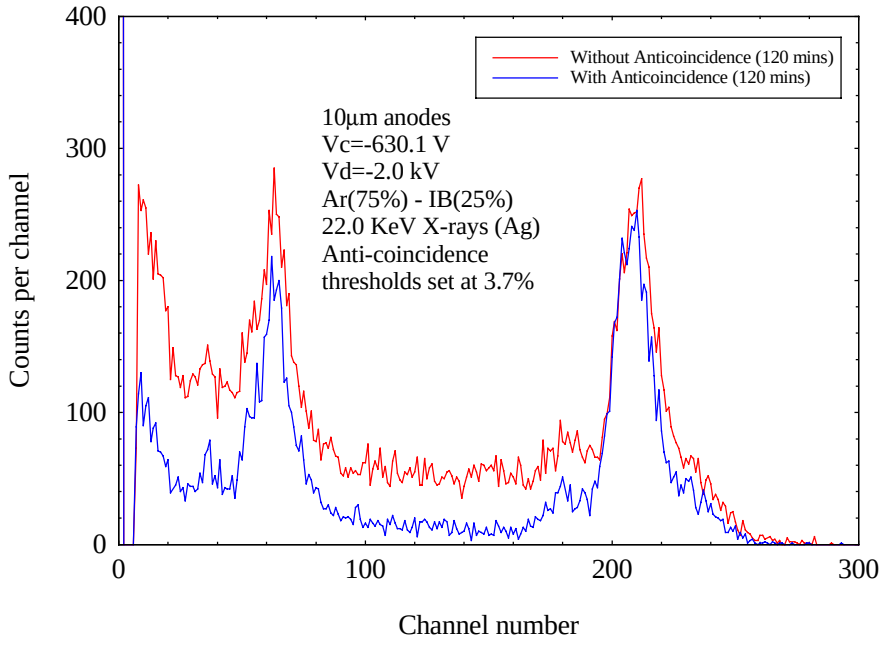

FIGURE 14

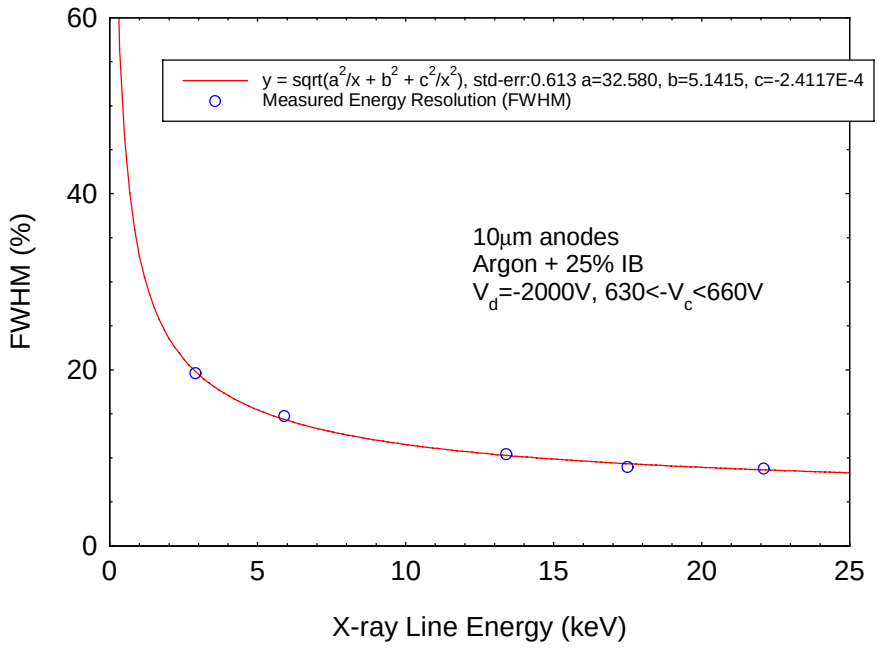
y = sqrt(a²/x + b² + c²/x²), std-err:0.613 a=32.580, b=5.1415, c=-2.4117E-4
Measured Energy Resolution (FWHM)
10μm anodes
Argon + 25% IB
V_d=-2000V, 630<-V_c<660V
FWHM (%)
X-ray Line Energy (keV)
0
20
40
60
0
5
10
15
20
25